SANDIA REPORT
SAND2014-19692
Unlimited Release
Printed November 2014

Progress and Improvements on Temperature Measurements for Dynamic and Advanced Certification Materials Experiments on Z

Tom Ao, Eric Harding, Jim Bailey, Dave Bliss, Dan Dolan, Marcus Knudson, John Benage

Prepared by
Sandia National Laboratories
Albuquerque, New Mexico 87185 and Livermore, California 94550

Sandia National Laboratories is a multi-program laboratory managed and operated by Sandia Corporation, a wholly owned subsidiary of Lockheed Martin Corporation, for the U.S. Department of Energy's National Nuclear Security Administration under contract DE-AC04-94AL85000.

Issued by Sandia National Laboratories, operated for the United States Department of Energy by Sandia Corporation.

Available to DOE and DOE contractors from
U.S. Department of Energy
Office of Scientific and Technical Information
P.O. Box 62
Oak Ridge, TN 37831

Telephone: (865) 576-8401
Facsimile: (865) 576-5728
E-Mail: reports@adonis.osti.gov
Online ordering: http://www.osti.gov/bridge

Available to the public from
U.S. Department of Commerce
National Technical Information Service
5285 Port Royal Rd.
Springfield, VA 22161

Telephone: (800) 553-6847
Facsimile: (703) 605-6900
E-Mail: orders@ntis.fedworld.gov
Online order: http://www.ntis.gov/help/ordermethods.asp?loc=7-4-0#online

SAND2014-19692
Unlimited Release
Printed November 2014

Progress and Improvements on Temperature Measurements for Dynamic and Advanced Certification Materials Experiments on Z

Tom Ao, Eric Harding, Jim Bailey, Dave Bliss, Dan Dolan, Marcus Knudson, John Benage
Dynamic Material Properties, Radiation and Fusion Experiments, and Imaging and Spectroscopy Groups
Sandia National Laboratories
P.O. Box 5800
Albuquerque, New Mexico 87185-MS1195

Abstract

Temperature measurements are very important in shock and ramp type dynamic materials experiments. In particular, accurate temperature measurements can provide stringent additional constraints on determining the equation of state for materials at high pressure. The key to providing these constraints is to develop diagnostic techniques that can determine the temperature with sufficient accuracy. To enable such measurements, we are working to improve our diagnostic capability with three separate techniques, each of which has specific applicability in a particular temperature range. To improve our capability at low temperatures (< 1 eV) we are working on a technique that takes advantage of the change in reflectivity of Au as the temperature is increased. This is most applicable to ramp type experiments. In the intermediate range (~1 eV< T< 5-10 eV) we are improving our optical pyrometry diagnostic by adding the capability of doing an absolute calibration as part of the diagnostic procedure for the shock or shock ramp dynamic materials experiment. This will enable more accurate temperature measurements for shock and shock ramp type experiments. For higher temperatures that occur in very high-pressure shock experiments, above 10 eV, we are developing the capability of doing x-ray Thomson scattering measurements. Such measurements will enable us to characterize strongly shocked or warm dense matter materials. Work on these diagnostic approaches is summarized in this report.

ACKNOWLEDGMENTS

We would like to thank the large team at Sandia that contributed to the design and fabrication of the loads and the fielding of the shock diagnostics for Z experiments. We also would like to thank the ZBL team for providing Z beamlet for the x-ray Thomson scattering experiments. We also thank the DICE team for helping with testing aspects of the reflectivity diagnostic and we greatly appreciate the help of the staff from NSTec that have contributed so much to the development of that diagnostic.

CONTENTS

FIGURES

INTRODUCTION

Understanding the properties and equation of state (EOS) of materials at high pressures contributes significantly to the stockpile stewardship mission of the NNSA laboratories and thus is an important component of many of the science campaigns funded by NNSA. In particular, the advanced certification program is tasked with understanding how many materials respond to dynamic compression at pressures up to 100's of GPa (10's of Mbar). Historically, much of this information was obtained through Hugoniot (shock driven) experiments. More recently, investigations are exploring a range of off-Hugoniot type experiments such as ramp compression and shock ramp compression. The material and EOS information obtained from these types of experiments generally involves determining the density as a function of the pressure, while the Hugoniot experiments determine the internal energy in addition to pressure and density. In general, the results from the experiments put fairly restrictive constraints on EOS models. However, the requirements placed on these EOS models by the stockpile stewardship program are severe and therefore improvements in the experiments are very valuable. One particular area where improvements can be made is in the measurement of the temperature of the material in the very experiments we have been doing. This is because many EOS models can reproduce these experiments and yet predict differing temperatures for the same pressure and density conditions. A temperature measurement that can discriminate between such models will lead to models that are more accurate, especially at conditions that vary from the measured conditions. With this as a goal, we have embarked on the development of multiple diagnostic approaches to measure temperature in a range of dynamic materials experimental conditions. Specifically, we seek to measure temperature for ramp, shock ramp, and shock experiments on a wide range of materials up to very high pressure conditions. The temperature range of interest is from ~ 1000 K (~ .1 eV) up to temperatures greater than 10 eV. The progress on these temperature diagnostic projects and the development of their usefulness on Z is documented in this report, which represents a component of satisfying an ACP level II milestone for FY14.

1. Low Temperature measurements using dynamic reflectance

High-speed temperature measurements are generally challenging, but states below a few thousand degrees K are especially difficult to characterize. Optical pyrometry is impractical in this domain because the emission levels are too weak for measurements that occur on the time scale of our ramp experiments; electrical gauges (thermocouples/thermistors) do not respond on these time scales and are difficult to use in harsh electromagnetic environments. These limitations are particularly troublesome in ramp-wave compression experiments such as in our cylinder experiments, where thermal measurements are extremely valuable but temperatures rarely exceed 1000 K.

Sandia has been working on an alternative method for measuring temperature in ramp-wave compression. Instead of relying on light emission from a sample, one can infer temperature based on how the sample reflects light. This technique can be applied to virtually any material, but gold is most convenient for high-speed measurements. Figure 1 shows how the reflectance of gold varies across the visible spectrum: long wavelengths are strongly reflected while short wavelengths are absorbed. The shape of the reflectance curve changes with sample temperature.

As gold is heated, its reflectance increases at short wavelengths and decreases at long wavelengths. Although reflectance changes at a particular wavelength can be subtle, the overall shape change is noticeable even at low temperatures. A streaked spectroscopy measurement of an embedded gold sensor illuminated by a white light source can provide real-time temperature measurements during ramp-wave compression. Gold has an extremely high thermal diffusivity (10^{-4} m^2/s) and does not form insulating oxides, so a 300 nm sensor equilibrates with its surroundings over a few nanoseconds.

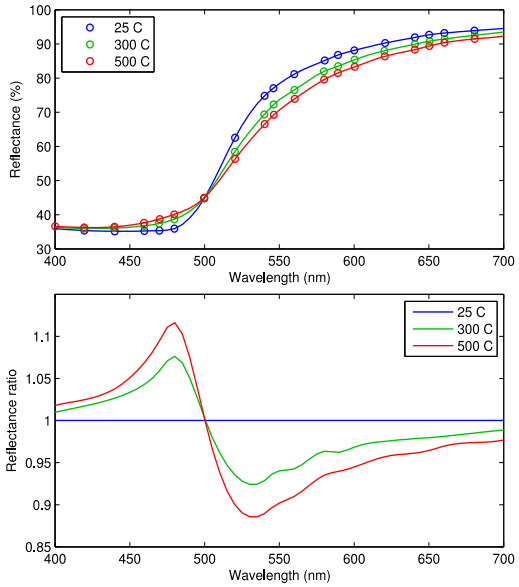

Figure 1: Reflectance (above) and reflectance ratio (below) spectra for gold at zero pressure

Calibration is crucial for the deployment of thermoreflectance sensors in dynamic compression experiments. The reflectance of gold (or any other material) is a function of both temperature and density/pressure, and the separation of these effects is not trivial. Measurements are made of the reflectance ratio (relative to the ambient state) spectrum, while thermodynamics affects the complex-valued dielectric/conductivity spectrum. Reflectance is also perturbed by the local dielectric index: a gold sensor viewed through a window is qualitatively different than a free surface measurement.

A minimal model for the optical properties of gold has been developed to handle these issues. This model uses six parameters to represent bound and free electron effects in gold at a particular temperature/density state; most gold models have ten or more adjustable parameters. Combining heated ellipsometry (at zero pressure) and diamond anvil cell measurements, the temperature and pressure variation of these parameters has been characterized up to 300 C and 30 GPa. Figure 2 shows how calculated reflectance ratio spectra compare with measurements from a heated impactor experiment [Dolan et al, Rev. Sci. Instr. **85**, 076102 (2014)], where equilibrium sensor temperatures and pressures are known independently. Quantitative agreement between model predictions and experimental measurements has been achieved, and refinements to the model should allow conversion of measured spectra to an inferred temperature-pressure state.

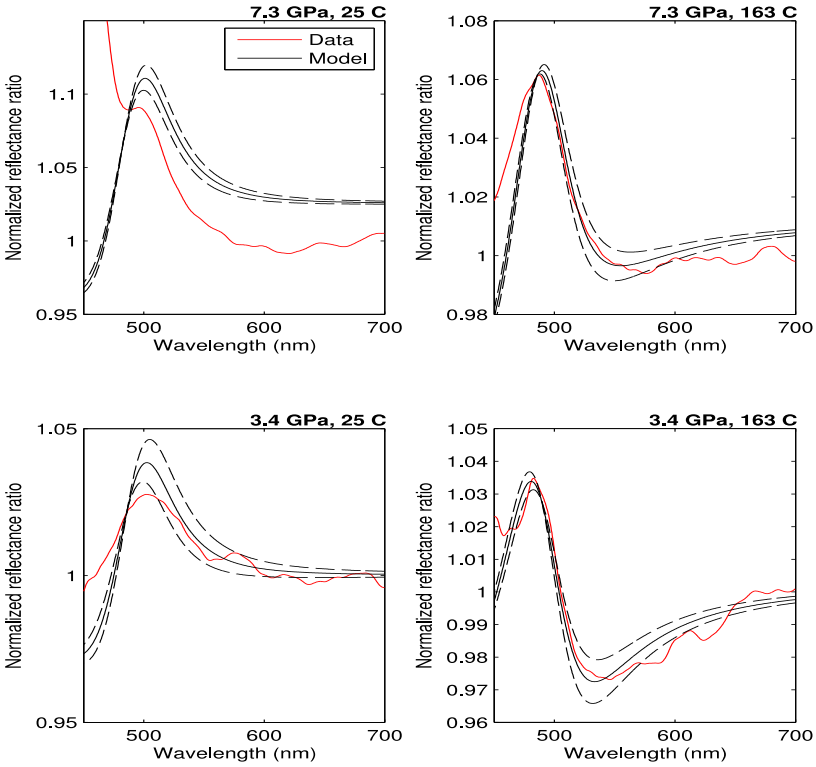

Figure 2: Reflectance ratios (red) for gold sensors under heated impact. Black lines indicate model predictions based on equilibrium sensor temperature; dashed lines indicate ±20 K variations.

Sample illumination is another key challenge in dynamic reflectance measurements. One possibility is to use light generated during the experiment. For example, stripline experiments on the Sandia Z machine are known to emit a significant amount of visible light; this emission is thought be related to stray current flow from the unconfined magnetic fields of the stripline. Several Z experiments have been performed with samples containing a metallic reflector, which reflect stripline emission into a probe. To test the feasibility of this diagnostic on Z, a specific prototype experiment was designed and fielded as part of the diagnostic suite for a liquid deuterium shock ramp experiment, Z2680. The results obtained indicate a very high level of data return and Figure 3 shows preliminary results obtained with a gold reflector; reference measurements are not currently available for converting intensity to reflectance. The reference measurements are a key requirement. Thus, a better light source, one with a known and reproducible spectrum, must be developed.

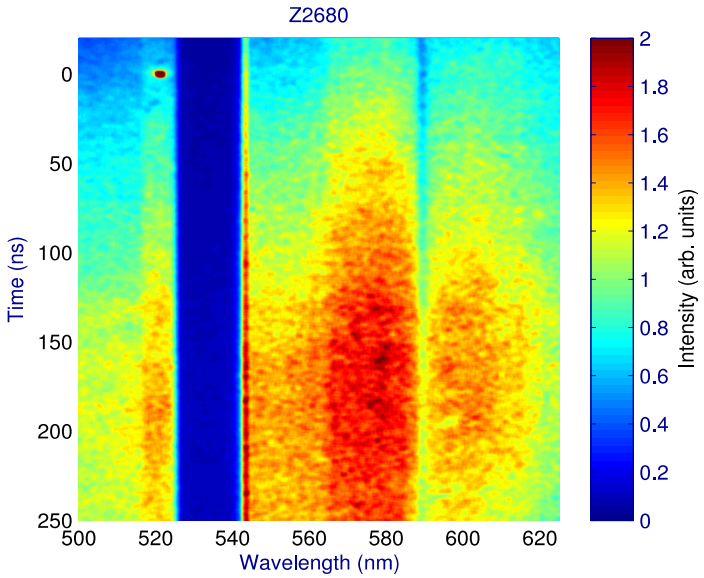

Figure 3: Streaked reflectance measurement for a liquid D_2 shock ramp experiment at pressures ~ 300 GPa. The dark region around 530 nm is due to a notch filter used to protect the streak camera from the VISAR

To address this issue, a variety of controlled light sources have been investigated. Several exotic solutions---such as laser-driven light sources and supercontinuum lasers---were tested, but xenon flash lamps have been found to be the best choice. Lamp geometry and plasma temperature are critical for overwhelming line emission with continuum radiation. Large-scale devices, such as the "MegaSun" system borrowed from NTS, have smooth emission spectra but are very difficult to use. Building on the integrating-sphere project from NSTec's Special Technologies Laboratory, we discovered many camera flashes have emission spectra and power output suitable for the type of streak camera measurements done for these experiments. Figure 4 shows a sample measurement from a $60 flash designed for a single-lens reflex (SLR) camera. The optical radiance generated by this lamp is sufficient for reflectance measurements in gun and Z experiments.

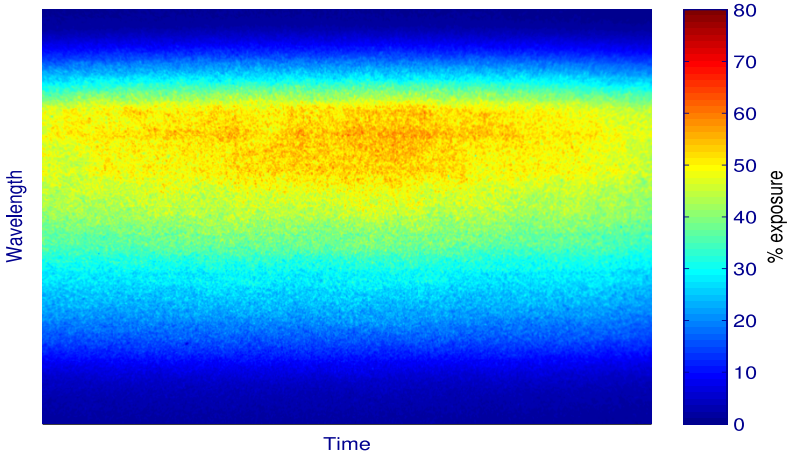

Figure 4: Streaked spectrum from a camera flash over 1000 ns (left to right) covering the visible spectrum (~400-700 nm from top to bottom).

Preliminary designs utilizing this particular flash are being developed and Figure 5 shows a mockup of how the camera flash would be used in the Z target chamber. The flash is powered by four AA batteries, which are sealed inside a separate container for use in millitorr to microtorr vacuum environments. The lamp is triggered by an infrared light pulse, which can be generated from a local diode or by a remote source over optical fiber. This setup has already been successfully tested in vacuum. A plastic light pipe (6-10 mm diameter) collects/homogenizes emission from the flash and delivers light to the sample. Laboratory tests indicate that the light pipe acts as a Lambertian source, similar to an integrating sphere, which minimizes tilt/motion effects in reflectance measurements. The light pipe approach is better suited to Z experiments---where samples are typically small and often cryogenically cooled---than an integrating sphere would be. Multiple light pipes can also be driven from a single flash. This preliminary design continues to be tested and improved and will be fielded this coming year on Z. The optimization of this light source and better characterization of gold reflectivity should lead to an improved diagnostic approach to low temperature measurements on high pressure ramp compression experiments in the near future.

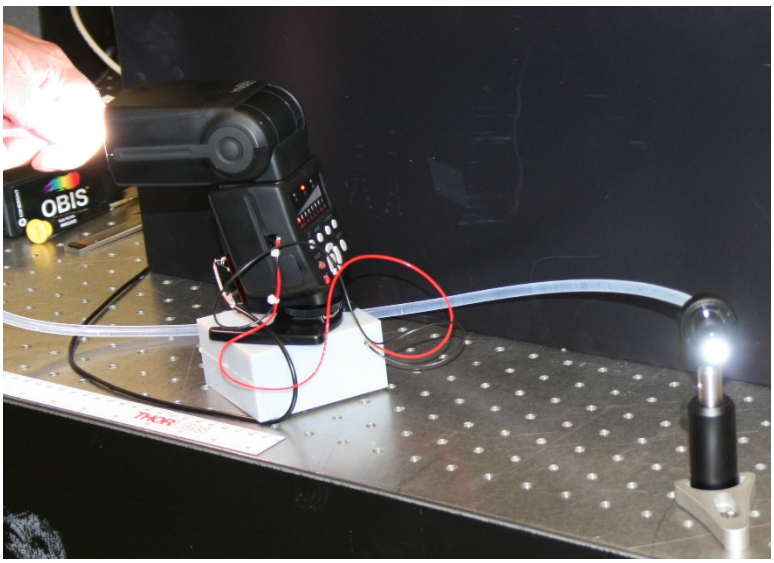

Figure 5: A plastic light pipe, illuminated by a commercial camera flash, serves as a low-cost, extended white-light source for reflectance measurements.

2. Moderate Temperature measurements using optical pyrometry

Optical pyrometry can be a useful technique for determining temperature at 0.5-10eV. [K. Falk, et al, PRE 90, 033107 (2014); C. Dai, et al, JAP **106**, 043519 (2009); D. Batani, et al, Laser and Particle Beams **31**, 457 (2013).] These are conditions typical in most shock and shock ramp experiments on Z and are applicable to many materials. The diagnostic tool used to obtain this type of data on Z is streaked visible spectroscopy (SVS). This technique enables one to obtain a time-dependent spectrum measurement from the sample. Then the spectra can be used to infer sample temperature *T* using the Plank equation.

$$\frac{dL}{d\lambda} = \varepsilon \frac{2hc^2}{\lambda^5 \left(e^{hc/\lambda kT} - 1\right)} \tag{1}$$

The spectral radiance $dL/d\lambda$ describes the amount of power emitted by the sample per unit area per unit solid angle per unit wavelength. A critical first step in pyrometry measurements is determining the relationship between the measured signal and the spectral radiance. Ideally, an absolute calibration is used to link a measured signal (CCD counts or film exposure) to a physical scale (watts/m^2/steradian/nm). However, absolute calibrations are generally not done because they are very time-consuming and require very careful measurements of every component in the diagnostic instrument. Relative calibration, where measurements at different wavelengths are proportional to radiance by a common scaling factor, are more common and can be useful in some settings for determining a 'color' temperature based on the slope of the emitted spectra. However, the slope does not constrain temperature nearly as well as the absolute radiance. Another possibility is to use a reference standard that is a component of the experiment and will emit sufficient visible light to enable a calibration to be done. A common reference in dynamic, transient experiments is quartz and this has been used on some Z experiments. The limitation in this approach is the accuracy of the standard, which typically is not as good as more common standards. We have decided to move forward on developing an absolutely calibrated system and we will also compare our new system to results obtained using quartz.

2.1 SVS Calibration Procedure

In this section we describe the process we use for absolute calibration of the SVS systems at Z. A multi-stage approach is required, taking special care to link each stage into a complete calibration. Figure 6 shows the conceptual layout for a pyrometry measurement using SVS.

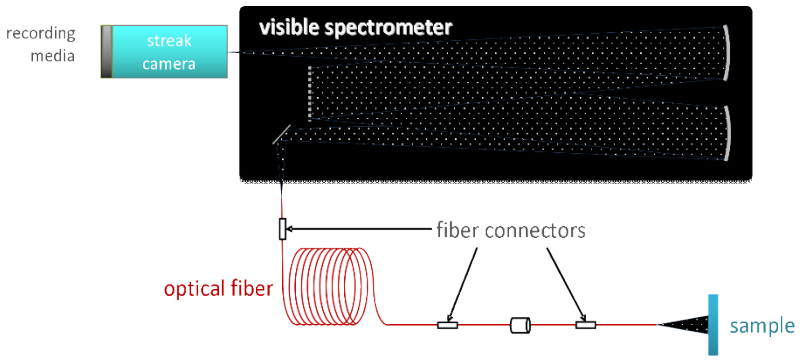

Figure 6. Conceptual layout of an SVS measurement.

An optical probe that may be as simple as a bare fiber tip collects light emitted from a sample. An important assumption is that the sample overfills the probe with a uniform radiance. When this is true, the sample-probe distance plays no role in light collection, resulting in constant signal levels for constant sample radiance. More precisely, the spectral flux collected by the pyrometry probe is a constant integral over angle and area.

$$\frac{d\Phi_1}{d\lambda} = \int d\Omega \int dA\ G(r,\theta,\phi)\frac{dL}{d\lambda} \approx Q(\lambda)\frac{dL}{d\lambda} \tag{2}$$

The geometric collection factor $Q(\lambda)$ is proportion to the collection area of the probe and the square of the numerical aperture of the probe. The spectral variation of $Q(\lambda)$ is typically weak but is accounted for in the calibration process so it is retained here for generality.

Light collected by the probe passes through a series of optical fibers. Some of this fiber resides in the center section of Z and is consumed during the experiment. The larger remaining portion of the fiber run is reusable, carrying light from the Z high bay to the SVS systems. The fiber is high-OH silica for best transmission in the visible with either a 100 or 200 μm diameter core. About 50 m of fiber including either one or two fiber connections are involved in this process. The spectral flux exiting the final jumper is related to the spectral flux collected by the probe as follows.

$$\frac{d\Phi_2}{d\lambda} = F(\lambda)\frac{d\Phi_1}{d\lambda} \tag{3}$$

The total fiber transmission, which includes the long transit fiber run plus any feed-throughs or jumpers and the associated connection losses, is collected into a single efficiency $F(\lambda)$. Note that spectral variation in fiber transfer can be quite significant, particularly for wavelengths below 450 nm.

Light entering the SVS is dispersed spectrally with a grating and temporally with a streak camera, creating a two-dimensional image where time t varies along one axis and wavelength λ varies along the other. The spectral flux exiting the final fiber enters the SVS system and passes through several stages: Spectrometer→Streak Tube→Phospher→MCP →Readout. Without

considering the underlying details, the transformation of spectral flux to readout signal $s(\lambda)$ can be viewed as a two-dimensional convolution.

$$s(\lambda,t) = \int dt' \int d\lambda' \; \eta(\lambda-\lambda', t-t') \frac{d\Phi_2}{d\lambda'} \approx C(\lambda,t) \frac{d\Phi_2}{d\lambda} \tag{4}$$

Assuming that light input varies slowly over the time/wavelength resolution of the SVS system the mapping of spectral flux to measured signal is a two-dimensional function. Combining equations 2 through 4, the measured SVS signal is related to spectral radiance by

$$s(\lambda,t) = C(\lambda,t) \; F(\lambda) \; Q(\lambda) \; \frac{dL}{d\lambda} \,. \tag{5}$$

In principle, one could expose the probe to a known spectral radiance and calibrate the SVS signal response in a single step. Unfortunately, this is not practical. Many measurements at Z create temperatures well in excess of 10,000 K – no calibration source could possibly mimic those light levels for calibration, particularly considering the requirement that the probe be fully filled. A further complication is that the functions C, F, and Q can vary from one shot to the next and need to be calibrated on every experiment. The time window for characterizing these efficiencies is severely constrained by the daily shot schedule so calibrations must be performed quickly.

Rather than measuring the $C(\lambda,t)$, $F(\lambda)$ and $Q(\lambda)$ functions independently, it is experimentally convenient to separate the problem into two contributions. The first contribution, $F(\lambda)\,Q(\lambda)$, describes the mapping of spectral radiance at the probe to spectral flux at the SVS input. The second contribution, $C(\lambda,t)$ describes how spectral flux entering the SVS maps to output signal. The combination provides an absolute calibration of the SVS measurement.

The intermediate calibration of the probe and fiber efficiency, $F(\lambda)Q(\lambda)$ requires a broadband source with a well characterized spectral radiance. The intermediate camera calibration $C(\lambda,t)$ requires a source with known spectral flux. Both sources must also be calibrated themselves over the full spectral range of interest. To measure $F(\lambda)Q(\lambda)$, the radiance source does not have to be extremely bright. However, to measure $C(\lambda,t)$ the flux source must have sufficient power to expose the streak camera at shot settings. For our broadband source of white light, we selected a commercially available unit from Energetiq, their fiber coupled Laser Driven Light Source (LDLS). The LDLS is used as the source for both measurements. When the LDLS output fiber is coupled directly into the SVS input slit it has sufficient spectral power to expose the streak camera. When the LDLS is coupled into a 2" diameter, integrating sphere, the inner surface of the sphere serves as a uniform, spectral radiance source that fully fills all modes of the probe fiber.

Fiber coupled, time-integrated spectrometers are a critical part of the intermediate calibration process. They allow the calibration process to proceed quickly on shot day by characterizing the collection efficiency of the probe and the fiber transmission in a single measurement. Previously, on shot day, the fiber efficiency, $F(\lambda)Q(\lambda)$, was measured with a power meter and a set of 22 individual band pass filters (BPFs). The procedure could take over 60 minutes to complete. Now, on shot day, it takes about 15 minutes to perform the two intermediate calibrations. The BPFs are still used to calibrate the small fiber spectrometers but are not required on every shot. Those calibrations are done offline with NIST traceable power meters.

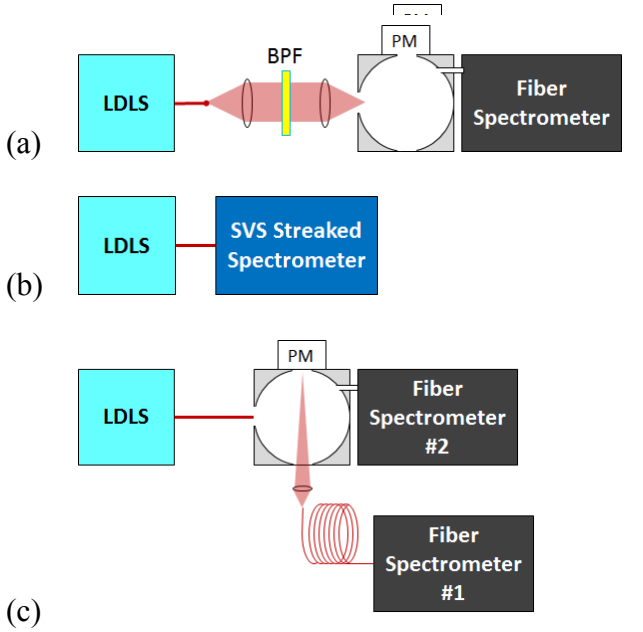

Figure 7. Schematic layouts of the various intermediate calibration steps are shown.
(a) Initial calibration of the fiber spectrometer, LDLS source and integrating sphere with a BPF set. A second PM is repeatedly inserted to measure the LDLS input power into the integrating sphere,
(b) Spectral flux calibration, $C(\lambda,t)$ of the SVS system.
(c) Spectral radiance calibration of the probe collection efficiency and fiber transmission $F(\lambda)Q(\lambda)$.

Based on testing we performed previously, the StellarNet Black Comet was selected as our compact spectrometer because it shows the best exposure linearity compared to Thorlabs and Ocean Optics units. Figure 7(a) shows a schematic layout of the measurement geometry used to calibrate the fiber spectrometer with the BPFs.

On shot day, two compact fiber spectrometers are used to make three measurements to calibrate the SVS system. Figure 7(b) shows the SVS system exposed to the LDLS source to calibrate $C(\lambda,t)$. Immediately after exposure, the spectral flux of the LDLS source is characterized by shining the source into the integrating sphere and recording the spectrum with the Stellarnet spectrometer.

Figure 7(c) shows the geometry used to calibrate $F(\lambda)Q(\lambda)$. The LDLS source, sphere and fiber spectrometer #2 are brought to the center section where the experimental probe to be calibrated is connected to a port on the integrating sphere. Fiber spectrometer #2 monitors the spectral radiance inside the sphere. Fiber spectrometer #1 located back in the SVS room, measures the spectral flux collected by the probe and transit fibers.

2.2 Application to Z Experiments

Calibration of SVS1 data on shot Z2582 is shown in figure 8. This particular shot was looking at high pressure GDP produced by a strong shock. These images show the visible emission from the target as a time-varying intensity. This is typical data obtained with the streak camera and has time going from top to bottom. Longer wavelengths are to the right. Figure 8(a) shows the

exposure of SVS1 to the LDLS as a pre-shot calibration. Figure 8(b) shows the calibrated shot data. The bright horizontal bands in the image are due to emission from the quartz windows. The dimmer region between the quartz bands at times from 220 to 240 ns corresponds to emission from the GDP. Figure 9 shows a plot of the spectral brightness averaged over the time period from 135-145 ns, which represents emission from the shocked quartz window but avoids the wavelength and timing fiducials and the blocking filter used to stop the VISAR laser. The best fit to this data corresponds to a temperature of 17,000 K with an emissivity of 0.45.

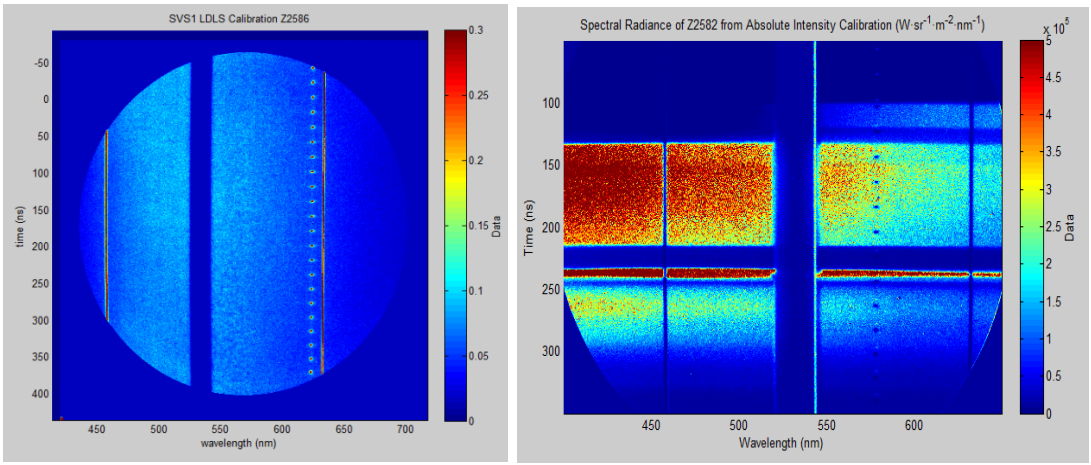

(a) (b)

Figure 8. SVS1 Data for shocked GDP. (a) Streak image of the LDLS calibration source. (b) Shot data corrected for the streak camera response.

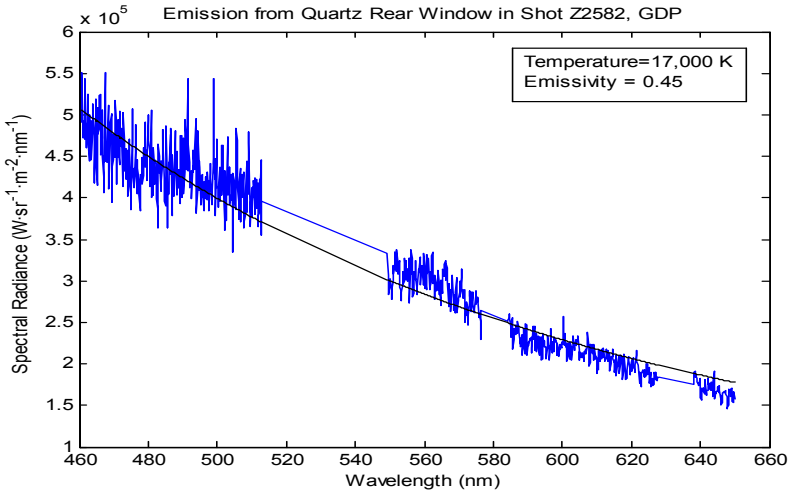

Figure 9. Fit to spectral response of emission from quartz window. The blue curve is the data from 135 to 145 ns in figure 8b and the gray curve is the fit to the intensity and spectrum.

As the process to calibrate and reduce SVS data is further verified and becomes more automated, temperature determinations by streaked optical pyrometry can quantitatively be applied to a

variety of experiments on Z. The temperature of LiD and D_2 samples will be compiled and compared to temperatures derived from the relative emission of the quartz windows. Also the absolute intensity of the quartz emission should be studied on as many samples as possible to develop a database for temperature calibrations relative to quartz. The combined results should enable temperature measurements for a range of shock and shock ramp compression experiments on Z important for the ACP and C2 programs.

3. High temperature measurements using X-ray Thomson scattering

To address measurements of higher temperature materials, > 10 eV, Sandia is developing a new capability to measure scattering of x-rays from a sample material on Z. These temperatures are typical of extremely strong shock experiments with pressures greater than 10 Mbar, especially for materials such as liquids and foams. The conditions produced in such experiments are sometimes referred to as warm dense matter(WDM). This past year, a prototype XRTS diagnostic experiment was carried out at the Z-accelerator. In this experiment, a magnetically accelerated flyer plate launched a shock into TPX (CH_2) foam sample, which was probed with x-rays from a plasma generated by the Z-Beamlet laser (ZBL). We successfully recorded space-resolved scattered x-ray spectra from the foam regions ahead and behind the shock. In addition, we simultaneously recorded the source x-ray spectrum. To the best of our knowledge, this is the first experiment anywhere to successfully record this combination of signals. This, coupled with the uniform and steady shock conditions produced, is the first step in facilitating novel x-ray scattering investigations of warm dense matter at the Z facility. The key achievements of the Z-XRTS work are summarized in this section.

We are interested in higher temperature measurements to address future experiments studying the properties of a range of materials at very high pressures. As mentioned above, many materials when shocked to such conditions reach a state often referred to as WDM. At such conditions, the temperature of the material is difficult to measure because it is too high for accurate optical measurements. X-ray Thomson scattering diagnostics overcome this dilemma because multi-keV x-rays penetrate into the plasma and provide a bulk measurement of the temperature. The term “X-ray Thomson scattering” is used in the literature [see, for example, Glenzer and Redmer, Rev. Mod. Physics **81**, 1625 (2009) and references therein] to refer to the combination of processes that contribute to spectrally-resolved scattered photon observations. The processes include Compton (inelastic) and Rayleigh (elastic) scattering for large wave number scattering and plasmon and Rayleigh scattering features at small wave number scattering. A variety of analysis methods exist and which method is appropriate depends on the material conditions. A unifying theme is that the density, temperature, and ionization information can be extracted from the scattered features.

The motivation for this work arises from the conjunction of two progress streams in high energy density physics. First, experiments on Z have demonstrated the ability to produce warm dense matter samples with unprecedented uniformity, duration, and size. However, the measurements to date have been limited mainly to density and pressure. Temperature measurements have been performed only on transparent samples that are compatible with optical emission diagnostics. Thus, the temperature information that is essential for completion of the equation of state is missing for many materials. The second progress stream is the development of x-ray probe

diagnostics on optical laser facilities. These experiments have demonstrated remarkable promise for diagnosing internal sample conditions using x-ray scattering and diffraction methods. However, they have been unable to provide benchmark quality material property measurements because the sample conditions are non-uniform and the sample evolution is too rapid.

In CY2013 and CY2014, a set of Dynamic Materials Properties (DMP) experiments on Z was performed to commission the XRTS capability. The goal of these experiments was to implement this complex technique on Z and demonstrate the ability to measure a scattered x-ray signal from a shocked warm dense matter sample. Using Z to create these conditions has some major advantages over laser facilities, namely that the samples are well-characterized, very uniform, and mm rather than micron size. These enable better analysis of the scattering data, provided the scattered signal is large enough. The overall experimental setup is shown in Fig. 10. The three key components of the Z-XRTS experiments are (1) the Z-DMP load, (2) the Z-Beamlet laser (ZBL), and (3) the x-ray scattering spherical spectrometer (XRS3). As shown in Fig. 11, ZBL irradiates a x-ray source place near the back surface of a sample. The x-rays penetrate the shocked sample and scatter out the side of the sample. The XRS3 diagnostic is setup perpendicular to the shock propagation direction to collect x-rays scattered from both shock and ambient states of the sample, and incident x-rays. This allows the uniformity of the WDM state to be verified, and the x-ray probe spectrum to be characterized simultaneously.

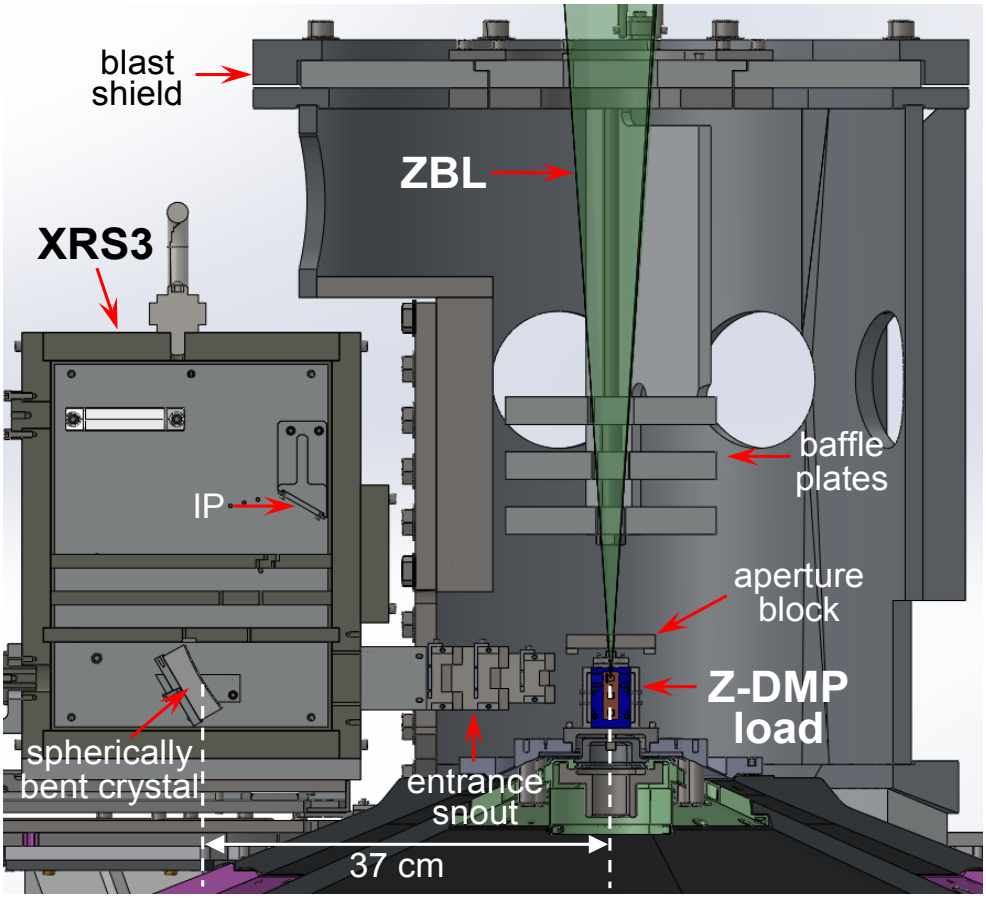

Figure 10. Experimental configuration for X-ray Thomson scattering measurements.

The Z-DMP coaxial load consists of two anode panels arranged around a central cathode stalk to form two anode-cathode vacuum gaps. The current J flowing on the anode and cathode produces a planar magnetic field B between them, and the J × B interaction results in a smooth mechanical stress wave that is proportional to the current squared. The generated impulsive pressure provides sufficient momentum to launch the aluminum anodes panels at high velocities across a gap and impact load samples. To reduce possible damage to ZBL, initial Z-XRTS experiments were restricted to low Marx charges of 53 kV, which generated Al flyers with peak velocities of only 16 km/s. In the later Z-XRTS experiments, a higher Marx charge of 85 kV was permitted, which enabled the launching of a solid Al flyer to a peak velocity of 25 km/s to impact a TPX (CH_2, 0.12 g/cm^3) foam sample (7.5 mm tall × 5 mm wide × 2.5 mm thick). The shocked CH_2 (0.75 Mbar, 4.3 eV, 0.52 g/cm^3) WDM state has large spatial extents along the shock propagation and lateral directions, and long steady-state duration (85 ns) that will be highly accessible for probing by the XRS3 diagnostic.

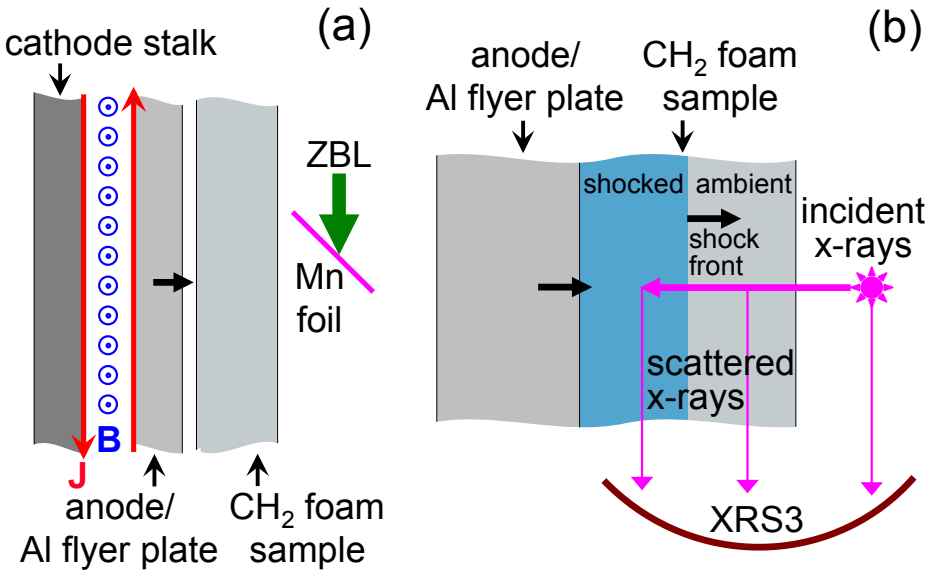

Figure 11. Experimental geometry showing position of backlighter target in a) and imaging orientation of x-ray spectrometer in b).

The ZBL beam is transported to the top of the Z center section chamber, passes through the final optics assembly (FOA) consisting of a turning mirror and a 3.2 m focal length lens, and enters the Z-DMP load region through a hole in the blast shield top lid. Inside the blast shield, the ZBL beam passes through three baffle plates and an aperture block above the Z-DMP load, before being focused onto the x-ray source target. The x-ray source target is fabricated from a 5 μm thick manganese (Mn) foil backed by a 100 μm thick layer of polyester. ZBL is optimized to provide 2 kJ of laser energy (λ = 527 nm, 0.5 ns pre-pulse, 2 ns main pulse, focused to ~ 2 × 10^{15} W/cm^2) to generate the bright Mn-He-α (6.181 keV) emission for XRTS. The firing of ZBL is timed so x-rays are generated 70 ns after the flyer impacts the CH_2 foam and 15 ns before the shock-breakout. With a 25 km/s Al flyer impacting a 2.5 mm thick CH_2 foam sample, the x-rays penetrate into sample when the shock wave, moving at a shock velocity of 29 km/s, has propagated 2.0 mm through it, so that 0.5 mm of foam remains ambient ahead of the shock front.

This enables simultaneous scattering from the 0.5 mm thick layer of shocked CH_2 foam, and from the 0.5 mm thick region of ambient CH_2 foam.

The XRS3 is a focusing spectrometer with spatial resolution, in which collected x-rays are spectrally and spatially resolved by a spherically bent crystal, and recorded onto a Fuji-TR image plate (IP). The relative x-ray collection efficiency, spatial resolution, and spectral resolution of spherically bent quartz, mica, germanium, and pyrolytic graphite crystals were investigated using a Manson x-ray source. A spherically bent germanium 422 crystal is fielded in the Z-XRTS experiment because it had the best combination of spatial and spectral resolution and x-ray collection efficiency. The spherically bent crystal and IP are housed inside a 1″ thick tungsten box for debris and x-ray background shielding. An entrance snout consisting of chevron (V-shaped) plates is meant to deflect load debris from entering the XRS3 spectrometer. In addition, several 1″ thick tungsten internal crossover plates that only allow x-rays that are reflected off the crystal to reach the IP are used to further reduce x-ray background.

The two main experimental challenges for XRTS on Z are (1) x-ray background overwhelming the XRTS signal, and (2) damage from load debris. First, Z itself is a tremendous x-ray source, where photons with energies up to 10 MeV are produced in both the power feed sections and load region, thus sufficient signal-to-noise for the XRTS measurement needed to be validated. Second, Z is a very destructive environment, where about 2-3 MJ (an energy release comparable to a stick of dynamite) is deposited into the load hardware, which sends debris everywhere. The primary concern is vertically directed debris damaging the ZBL FOA and creating a catastrophic vacuum breach of the target chamber. Another concern is debris entering the XRS3 spectrometer and damaging the IP, thereby preventing retrieval of the XRTS data.

The XRS3 with its thick layers of tungsten shielding was designed to suppress the x-ray background, and was tested as a ride along diagnostic on several Z-DMP experiments. It was shown that Z-DMP experiments have significantly lower x-ray background than z-pinch experiments. The x-ray background at the bottom entrance of the XRS3 box where the spherically bent crystal sits was on order several PSL (photostimulated luminescence). This was further reduced by a factor of 30 using the internal tungsten crossover plates, so that at the IP only about 0.1 PSL x-ray background was measured. This modest x-ray background makes XRTS viable for Z-DMP experiments. The entrance snout deflected most debris from entering the XRS3, thus the image plate was undamaged and XRTS data was recovered. However, the spherical crystal was still damaged by the remaining undeflected projectiles, so additional shielding to protect the crystal is being investigated.

Currently, a sacrificial 10 mm thick glass debris shield is placed below the ZBL FOA window (30 mm thick glass) to stop any debris from reaching it. The debris mitigation strategy for the Z-XRTS experiment is based upon previous hypervelocity penetration depth studies of particle impacts on glass/vacuum interfaces. The penetration depth into the glass shield depends upon a projectile's mass density, size and velocity. Increasing the thickness of the glass shield would prevent perforation, but would decrease the focusing quality of ZBL. The alternative is to decrease the mass density, size, and velocity of projectiles reaching the glass shield. This was accomplished using an aperture block near the load and baffle plates above it within the blast shield to limit the axial debris. In initial commissioning Z-XRTS experiments, the ZBL FOA

was located outside of the Z center section vacuum chamber, so any damage to the window could result in a vacuum breach. In later Z-XRTS experiments, a new vacuum ZBL FOA chamber was used to further mitigate the possibility of a catastrophic vacuum breach.

In the first full commissioning Z-XRTS experiment (Z2474), Z was fired with a Marx charge of 53 kV in conjunction with 2 kJ of ZBL laser energy focused into the Z target chamber. However, there was large anomalous current loss away from the load that severely reduced the flyer peak velocity to only 9 km/s, which was much lower than the expected 16 km/s peak velocity. As a result, ZBL generated x-rays about 190 ns early relative to shock arrival in the CH_2 foam and scattering was only from ambient CH_2 foam.

In a subsequent Z-XRTS experiment (Z2568), the flyer reached a peak velocity of 15 km/s that was closer to nominal value. However, the generated x-rays were considerably weaker than those measured in the previous Z-XRTS experiment. A pinhole image of the Mn x-ray source showed not only a weaker signal than measured previously, but also a noticeable lateral asymmetry across the x-ray image. Spectral analysis of the very weak Mn x-ray source spectrum suggested the laser intensity was too low, consistent with only about 100-200 J of ZBL laser energy actually reached the Mn target. After careful review, it was suspected that plasma jetting from load was interfering with ZBL beam path.

For the next Z-XRTS experiment (Z2661), a Marx charge of 85 kV and the vacuum ZBL FOA chamber were used. In addition, the load hardware was modified to mitigate possible Z-DMP load and ZBL interaction issues that previously generated the very weak x-ray signal. It was hypothesized that early in time some leakage current at the small gap between top and bottom shorting caps produced plasma that disrupted the ZBL path to the Mn target. A new overhang feature on the top shorting cap was added to block/divert any plasma produced at the shorting gap, and appears to have work as designed. Specifically, the pinhole image of the Mn x-ray source captured was intense and laterally symmetric, indicating the ZBL path was unobstructed. The flyer velocity profile and peak velocity (25.4 km/s) measured by VISAR agreed well with the predicted shape and peak value (25 km/s) of the ALEGRA simulation. Finally, the XRTS data measured by XRS3 was quite definitive in spatially and spectrally resolving the shock and ambient states of the CH_2 foam sample, and the Mn x-ray source, as shown in Fig. 12. However, background levels and the complicated spectrum prevented a determination of the temperature. Future work will focus on improving the source spectrum and intensity and reducing the background. These efforts should lead to improvements that will better enable future temperature measurement for materials at WDM conditions.

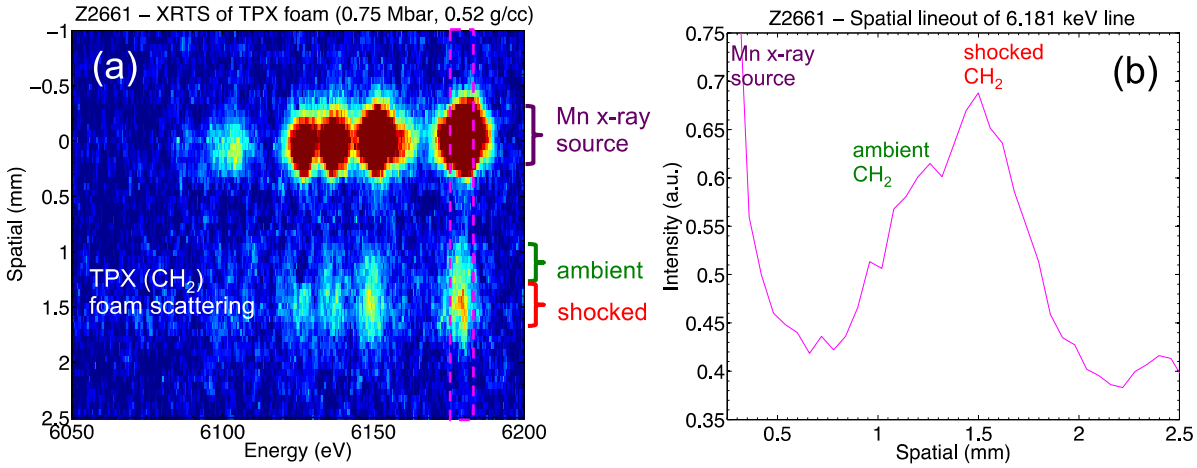

Figure 12. Image of x-ray scattering results from Z2661 in a) and spatial lineout from image at 6.181 keV in b).

5. CONCLUSIONS

We have completed a set of experiments to improve our temperature measurement capability on Z. These experiments include a prototype experiment measuring the reflectivity of Au on a shock ramp compression of deuterium, a prototype experiment measuring the x-ray scattering from a shocked low density foam demonstrating x-ray Thomson scattering in the warm dense matter regime, and the application of a new absolute calibration procedure for streaked optical pyrometry that has been fielded on several experiments and analyzed and documented on one of those experiments. The three techniques are aimed at enabling temperature measurements from well below 1 eV to temperatures above 10 eV. These results have enabled Sandia to meet the requirements of an ACP Level II milestone this year. We will continue to work on all three techniques to improve our temperature measuring capability and by doing so, improve the overall precision and relevance of our dynamic materials experimental program.

DISTRIBUTION

1	MS0899	Technical Library	9536 (electronic copy)


Sandia National Laboratories